Check for updates

Stability of lower limit of air pressure in abandoned coal mine roadways during long-term CAES

Jian Jiang[1], Pengyu Guo[2]*, Xiaokui Yu[1], Qili Lin[3], ZhiGuo Li[1], Jitao Wu[2] and Jianxun Wu[1,2]

[1]East China Electric Power Design Institute Co., Ltd. of China Power Engineering Consulting Group Co., Ltd, Shanghai, China, [2]School of Resource and Safety Engineering, Chongqing University, Chongqing, China, [3]Engineering Technology Institute for Energy Storage of China Power Engineering Consulting Group Co., Ltd. Shanghai, China

Power supply instability in the grid has been exacerbated by the rapid development of new energy generation methods. Notably, large-scale energy storage is the most practical solution to this problem. Meanwhile, in China, an effective method of reusing the increasing number of abandoned coal mines is urgently required. Accordingly, building compressed air energy storage (CAES) plants along the roadways of abandoned coal mines can serve as a viable energy storage method while repurposing these mines. This study examined the effect of the lower limit of air pressure (LLAP) on the stability of coal mine roadways in CAES applications by considering an ongoing pilot CAES coal mine in Chongqing, China. The findings indicate that the LLAP has a positive correlation with the roadway stability provided the frequency of air injection/extraction and upper limit of air pressure are constant. Over 10 years of CAES operation, a higher LLAP corresponds to less overall deformation of the roadway and top slab subsidence, and smaller plastic zone volume. Furthermore, the first main principle stress also decreases as the LLAP increases. According to the findings of this paper, the LLAP for the actual operation of CAES should be adjusted upwards as appropriate, which help to improve the geological stability of CAES roadways.

KEYWORDS

abandoned coal mine, CAES, lower limit of air pressure, roadway deformation, plastic zone, stability

1. Introduction

Climate warming has placed a major constraint on global economic development. Climate change is mainly being mitigated by reducing carbon emissions (Mathiesen et al., 2011; Zhang et al., 2016). Over the past few decades, fossil energy consumption has been on the rise, corresponding to a rapid increase in carbon emissions. Governments are becoming aware of the climate problem and are introducing a range of policies to reduce carbon emissions (Zhou et al., 2014; Zhao et al., 2017). The US government has implemented total control and carbon emissions trading to reduce greenhouse air emissions by more than 50% by 2050 (compared to 1990 amounts; Guerra et al., 2020). The EU's latest energy bill proposes an increase in the share of renewable energy in the total energy consumption to 45% by 2030, with photovoltaic and solar energy accounting for 40% (Liu et al., 2020). Japan's carbon neutrality bill states that Japan will be carbon neutral by 2050. In line with the goals of achieving peak carbon by 2030 and carbon neutrality by 2060, the latest document from the Chinese government outlines increasing the proportion of electricity generated from nonfossil sources beyond 39% by 2025

(Ran et al., 2023). In recent years, the adoption of new energy generation methods in China has been increasing, with wind power installations growing at an average rate of approximately 42%. In addition, China is rich in photovoltaic resources, with more than 66% of the country having more than 2,000h of total annual light, generating approximately 5,000 MJ/m^2 of light energy (Yu and Qu, 2010; Gao et al., 2022) (Figure 1).

New energy generation can effectively reduce carbon emissions, but power generation instability remains unresolved, becoming a major constraint to its development (Lund and Salgi, 2009; Qin and Loth, 2021). Large-scale energy storage is a viable solution to this problem. It involves storing excess electricity during periods of low electricity consumption and releasing it during peak consumption periods. Therefore, the combination of new energy generation and energy storage can provide a stable supply of electricity (He et al., 2019; Wu et al., 2020). Currently, the main energy storage methods are pumped hydrostorage (PHS), compressed air energy storage (CAES), and electrochemical storage (ES; Zakeri and Syri, 2015; Zhang et al., 2016). The construction of PHS stations has reached saturation due to geographical constraints and negatively impacts the environment, whereas ES has a low lifespan, and rational disposal of batteries remains an unresolved issueand. Comparing the different types of energy storage, we find that CAES is a more viable energy storage method (Lund and Salgi, 2009; Yang and Jackson, 2011; Kang et al., 2020).

CAES involves the compression and storage of air in underground caverns or pressure vessels, and the high-pressure air drives a turbine to generate electricity when it is needed (Kim et al., 2012; Apostolou and Enevoldsen, 2019). The Huntorf CAES plant in Germany and the McIntosh CAES plant in the USA utilise abandoned salt caverns, and Mandhapati has modelled and evaluated the heat and mass changes in the Huntorf plant (Mahlia et al., 2014; Chen et al., 2017). However, the rocks in most abandoned salt caverns in China are stratified salt with small salt thicknesses, and the volume of individual salt caverns formed after salt mining is small, making them inefficient for CAES applications (Guerra et al., 2020; Liu et al., 2020). The gradual decommissioning of abandoned coal mines has resulted in vast abandoned underground spaces. It is estimated that China will have launched 15,000 coal mines by 2030 (Luo and Chen, 2011; Cui et al., 2020; Fan et al., 2020a,b). Utilising abandoned coal mines can not only contribute to the development of new energy sources for the country but also reduce the environmental and safety problems associated with decommissioning abandoned coal mines (Wang et al., 2023). Javier et al. explored the feasibility of an integrated system for CAES, PHS, and thermal storage in abandoned coal mines (Menéndez et al., 2019). Fan et al. investigated the feasibility of compressed air storage in abandoned coal mines in China (Lutyński, 2017; Menéndez et al., 2019, 2020). Kim proposed the concept of shallow buried cave compressed air storage (Fan et al., 2020b; Figure 2). Wolf et al. investigated the feasibility of porous sandstone for compressed air storage under geological conditions (Pfeiffer et al., 2021). Zhou et al. analysed energy changes and air leakage during compressed air storage (Zhou et al., 2014). Liu et al. analysed the mechanical
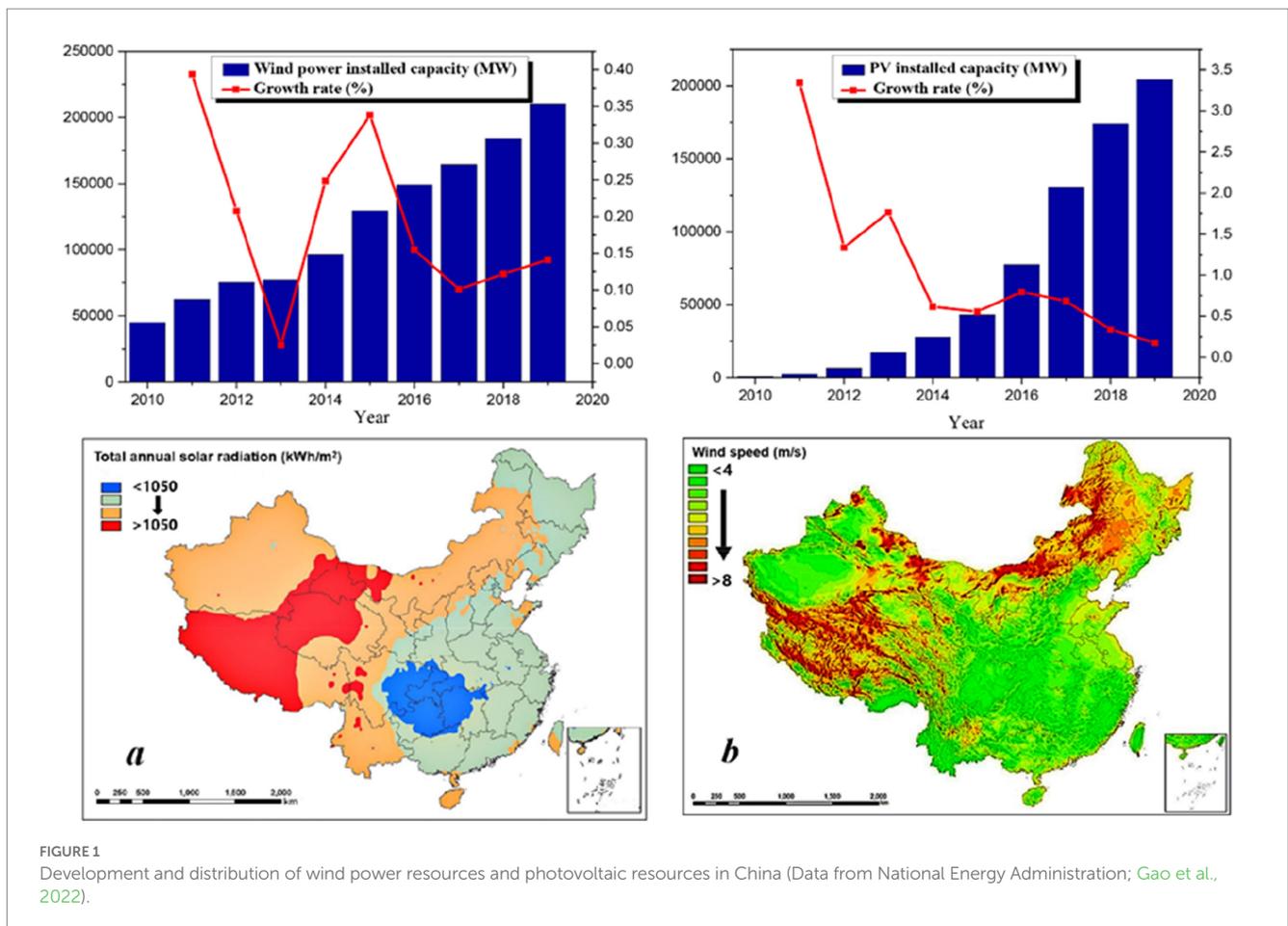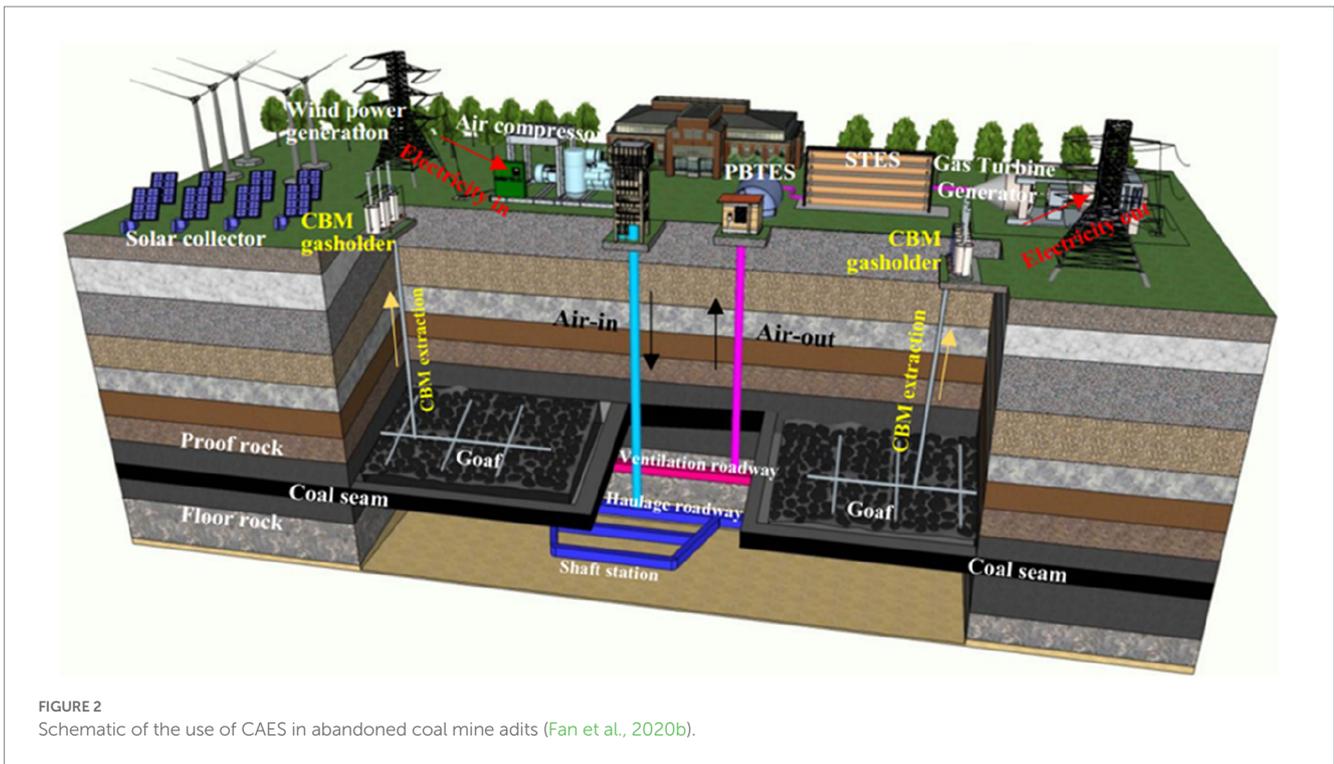

FIGURE 1
Development and distribution of wind power resources and photovoltaic resources in China (Data from National Energy Administration; Gao et al., 2022).

FIGURE 2
Schematic of the use of CAES in abandoned coal mine adits (Fan et al., 2020b).

properties and fatigue characteristics of concrete under complex stress paths to explore the stability of gas storage in abandoned coal mine roadways (Liu et al., 2022, 2023).

CAES has mainly been researched from thermodynamic and kinetic perspectives, with the stability of CAES storage in abandoned coal mine roadways being understudied (Fan et al., 2019; Li et al., 2022a,b). Although Falko et al. studied the effect of cyclic loading on the stability of abandoned coal mine roadways (Schmidt et al., 2020), the effect of roadway creep was not considered despite its significance. In this paper, the stability effects of different pressure ranges on the CAES of abandoned coal mine roadways are investigated by considering an ongoing CAES project in Chongqing. Moreover, the mechanical properties of the surrounding rock and the creep effect are considered (Fan et al., 2019, 2020).

2. Methods

2.1. A-CAES scheme and study area

All coal mines in Chongqing, China were decommissioned at the end of 2020. Chongqing recently initiated a research programme on energy storage in underground abandoned spaces. In this scheme, a pilot CAES for abandoned coal mines was established in Chongqing. Among the abandoned coal mines, the Datong No. 1 mine is the most prospective pilot site for the construction of CAES because it has the largest capacity, large underground waste space, and good geological conditions. Approximately 1,500, 000 m^3 of rock roadways of abandoned underground space were formed during the service life of the mine, including shafts, drifts, and liaison lanes. Abandoned roadways are the best storage sites for CAES owing to their larger storage space and stability. In this study,

two parallel roadways located at a depth of 300 m were selected as the air storage space: their total length and storage volumes are 5,000 m and 98,174 m^3, respectively. The surrounding rock of the stratum in which the roadways are located is sandstone, with the upper and lower parts being limestone. To improve the air tightness and stability of air storage in the lanes, they were lined with 30 cm of concrete.

2.2. Numerical model

FLAC3D was used for the numerical simulation, which is widely used for geotechnical finite element numerical simulation. The model was built and meshed using Hyper Mesh software. The length, width, and height of the model were 40 m, 30 m, and 40 m, respectively, and the total number of meshes was 131,687. A 10 m-thick limestone was situated above and below the model, whereas the rock layer where the roadways were located was 20 m sandstone. The shape of the roadways was modified to improve its stability during pressured air storage. The radius of the modified roadways was 2.5 m, and the distance between the two roadways was approximately 16 m (Figure 3). The perimeter and bottom of the model were fixed constraints, and the top was subjected to vertical stresses from the overlying rock layer, which are calculated as

$$P = \int_0^h \rho g h \qquad (1)$$

Where ρ is the density of the rock formation in kg/m^3, g is the acceleration of gravity in m/s^2, and h is the distance from the ground to the top of the model in m.
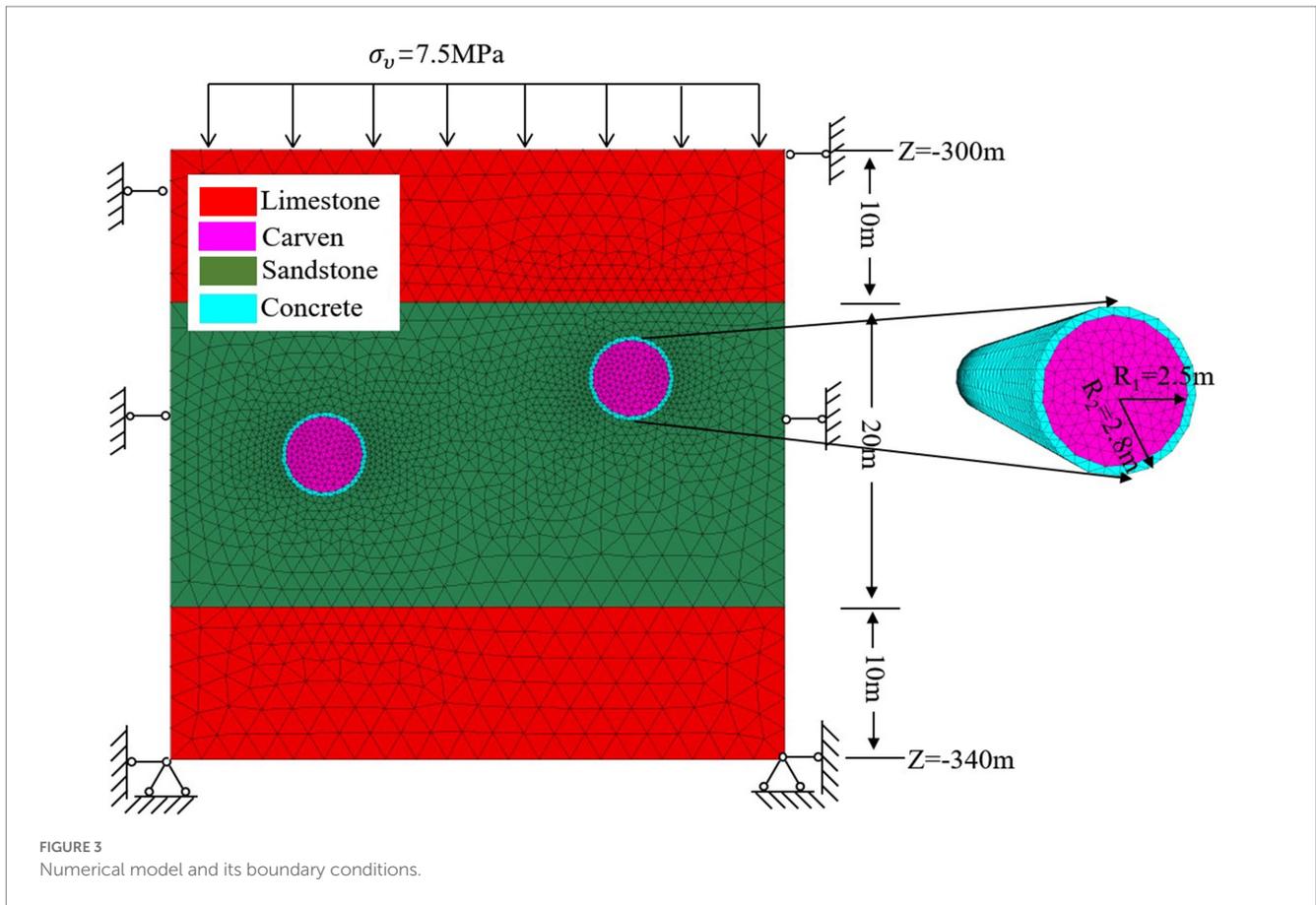
FIGURE 3
Numerical model and its boundary conditions.

TABLE 1 Model parameters used for modeling CAES plant operation.

Parameter	Concrete	Limestone	Sandstone
Unit weight, γ (kN.m^{-3})	2,300	2,500	2,530
Elastic modulus, E_i (Gpa)	25	32	36
uniaxial comp.strength, σ_{ci} (Mpa)	35	45	60
Poisson's ratio	0.16	0.3	0.2
Tensile strength (Mpa)	6	5	12
Cohesion (Mpa)	2	3	4
Friction angle (°)	45	50	53

The vertical stress generated by the overlying rock layer of the model was calculated as 7.5 MPa.

The Mohr–Coulomb linear elasticity–complete plasticity criterion was applied to the model as a whole, where plastic damage of the material occurs after the Moor failure strength has been reached. The Mohr–Coulomb plastic damage criterion is

$$\frac{1}{2}\left(\sigma_1 - \sigma_3\right) = c\cos\phi - \frac{1}{2}\left(\sigma_1 + \sigma_3\right)\sin\phi \qquad (2)$$

Where σ_1 and σ_3 are the maximum and minimum total principal stresses in MPa; σ_1 and σ_3 are the maximum and minimum principal stresses in MPa, respectively; φ is the friction angle in degrees; and c is the cohesion force in MPa.

2.2.1. Model mechanical parameters

The material parameters for the surrounding and overlying rock were obtained from the ongoing project, whereas the mechanical parameters for the concrete lining were obtained from Zhou et al. (2014). The specific parameters are listed in Table 1.

Concrete is a typical viscoelastic material. The Burgers creep model was chosen for the creep model to predict long-term concrete deformation. Notably, the Burgers body consists of a Maxwell body and a Kelvin element in series (Ma et al., 2022; Figure 4).

The principal equation of the Burgers model is

$$\begin{cases} \text{Maxwell}: \varepsilon_1 = \dfrac{1}{\eta_1}\sigma_0 t + \dfrac{\sigma_0}{E_1} \\[2mm] \text{Kelvin}: \varepsilon_2 = \dfrac{\sigma_0}{E_2}\left(1-\exp\left(-\dfrac{E_2}{\eta_2}t\right)\right) \\[2mm] \text{Burgers}: \varepsilon = \dfrac{\sigma_0}{E_1} + \dfrac{\sigma_0}{\eta_1}t + \dfrac{\sigma_0}{E_2}\left(1-\exp\left(-\dfrac{E_2}{\eta_2}t\right)\right) \end{cases} \qquad (3)$$

Where E_1 and η_1 denote the modulus of elasticity and viscosity coefficient of Maxwell's section respectively, whereas E_2 and η_2 denote the modulus of elasticity and viscosity coefficient of Kelvin's section, respectively.

$$\varepsilon(t) = \frac{\sigma_0}{E_1} + \frac{\sigma_0}{\eta_1}t + \frac{\sigma_0}{E_2}\left(1-e^{\frac{E_2}{\eta_2}t}\right) \qquad (4)$$
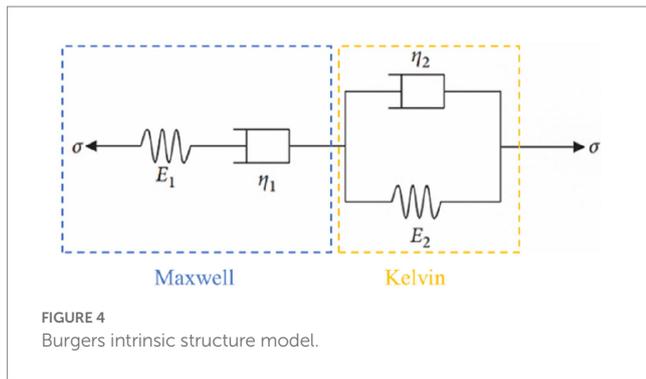
FIGURE 4
Burgers intrinsic structure model.

TABLE 2 Mechanical properties of the viscoelastic Burgers rock.

E_1 (MPa)	η_1 (MPa.year)	E_2 (MPa)	η_2 (MPa.year)
344.738	655.758	3447.379	131,200

Data from Goodman (1989).

Where σ_0 is the constant stress and t is load time.

In the finite element simulation, the creep parameters of concrete, in addition to its basic mechanical parameters, are required. Table 2 presents the creep properties of the Burgers model.

In addition, the creep effects of limestone and sandstone are not considered in this model. Additionally, the effect of air leakage on the internal pressure of the roadway during the pressure air storage process is ignored.

2.3. Simulation procedure

The stress field distribution of rock in deep underground space is approximated by hydrostatic stress, and the stresses are isotropic. Therefore, an isotropic stress field ($\sigma_{xx} = \sigma_{yy} = \sigma_{zz}$) is applied to the model as a whole during the simulation. The roadway excavation is assumed to be instantaneously completed and solved for the state of stress equilibrium regained after the roadway excavation.

After the roadway is formed, the displacement of the model as a whole is zeroed, concrete lining is added to the roadway, and the interior walls of the roadway are subjected to cyclic internal pressure. Considering that the CAES plant can be used as an emergency power source, charging and discharging processes are assumed to be performed once a month, with equal time intervals between each charge and discharge. Each charge/discharge cycle is 24 h, and the simulation time is 10 years. The air pressure variation is shown in Figure 5 (8 h for charging, 6 h for the upper pressure holding time, 4 h for discharging, and 4 h for the lower pressure holding time; Fan et al., 2020b). According to Liu et al., the general pressure range for salt cavern air storage is 40–80% of the *in-situ* stress (Liu et al., 2020). However, no relevant reference for the range of air storage in coal mine roadways exists. In this section, the upper limit of air storage pressure is kept constant at 80% of the *in-situ* stress, that is, 6 MPa, and different lower limit air pressures (LLAPs) of 3 MPa, 3.75 MPa, 4.5 MPa, and 5.25 MPa (40, 50, 60, and 70% of the *in-situ* stress, respectively) are selected as the research objects to analyse the effect of different air storage ranges on the roadway stability.

3. Results and discussion

This section analyses the changes in the stability of the roadway after 10 years of operating the CAES plant as an emergency power source. The amount of top slab subsidence at different pressure limits, the overall displacement of the roadway, and the plastic zone in the roadways are discussed.

3.1. Overall deformation of roadways

Figure 6 shows that the surrounding roadway rock is displaced to varying degrees under the action of *in-situ* stress and circulating air pressure. At a constant upper limit pressure, the lower limit pressure of the roadway is, the greater the displacement of the roadway. Under the influence of in-stiu stress, the surrounding roadway rock contracts toward the center. Under internal air pressure, the roadway rock expands in all directions. The greater the difference between the two is, the greater the contraction of the roadway. At a lower limit pressure of 3 MPa, the overall displacement of the roadways rock was approximately 10 mm: the top, bottom, and two gangs were displaced by 13 mm, 9 mm, and 11 mm, respectively. At a lower limit pressure of 5.25 MPa, the overall roadway displacement was approximately 3 mm, with the top and two gangs being displaced by 4 mm and 2 mm, respectively. At pressures of 3.75 MPa, 4.5 MPa, and 5.25 MPa, the displacements were 69, 54, and 23% of those at pressures of 3 MPa, respectively.

By and large, the magnitude of the displacement is positively correlated with the pressure difference (the upper and lower limits of air pressure during the pressure-air storage process in the roadway). This phenomenon is attributed to a low lower pressure limit corresponding to a greater common pressure difference between the internal pressure in the roadway and the *in-situ* stress. Additionally, the greater the pressure difference, the likelier the roadway deformation. Therefore, when the upper air pressure remains constant, the lower air pressure should be higher to ensure tunnel stability.

3.2. Amount of top slab subsidence

The analysis in the previous section reveals that the cumulative displacement of the roadway is negatively correlated with the lower pressure limit. Figure 7 shows the top slab displacement in the roadway. Eventually, the top roadway slab under all four working conditions produced varying degrees of subsidence. In general, the roof slab is more susceptible to damage than the bottom slab and both gangs. The top slab of the roadway subsided by approximately 1.3 cm at a lower limit pressure of 3.0 MPa and by approximately 2 mm at an LLAP of 5.25 MPa. These displacements correspond to each other and to the roadway displacements in Figure 6. The cumulative displacement of the top of the roadway signifies the creep in the surrounding rock. The magnitude of the deflective stress varies for different stress lower limit cases. Therefore, the cumulative top slab sinking increases with LLAP.
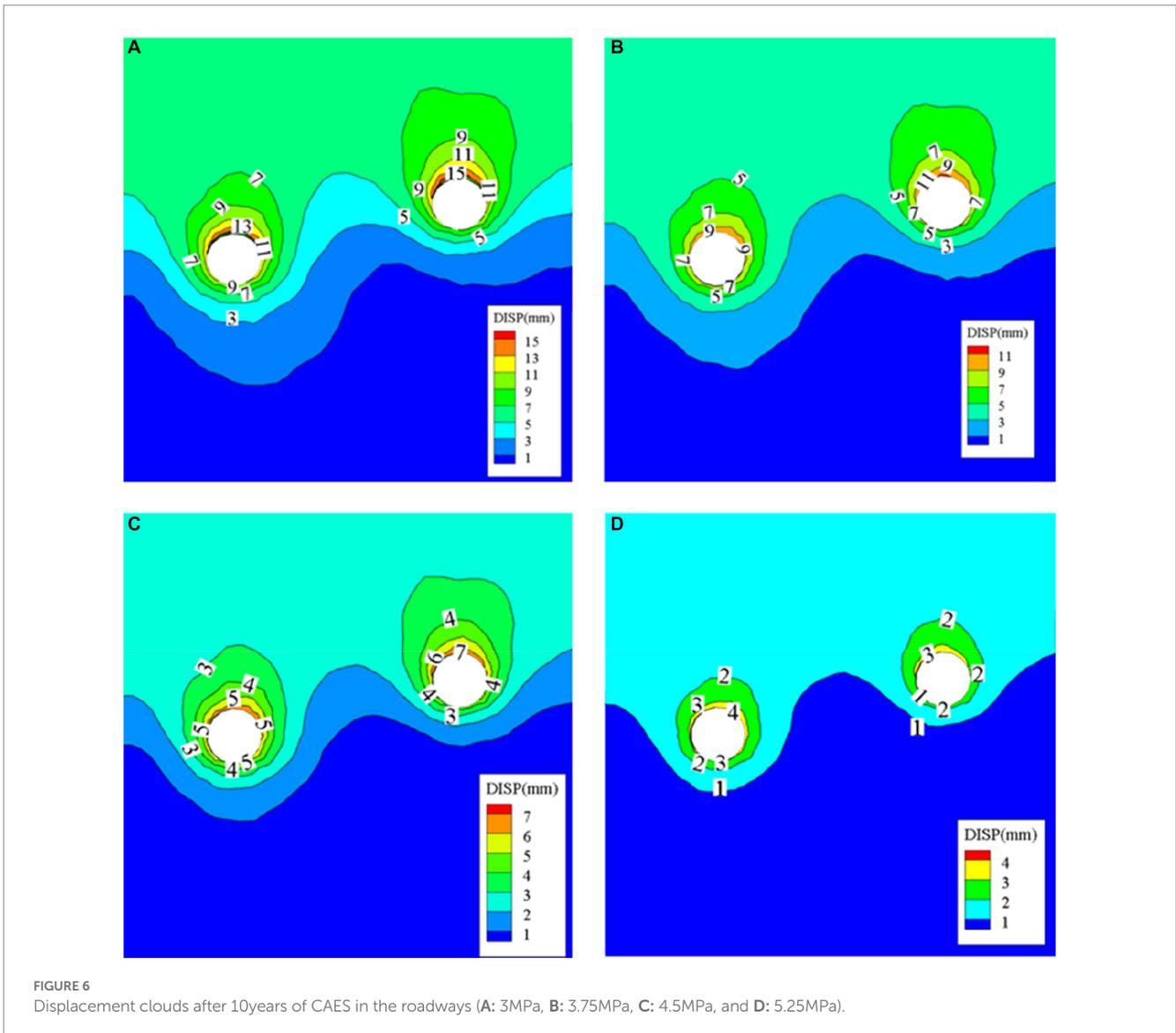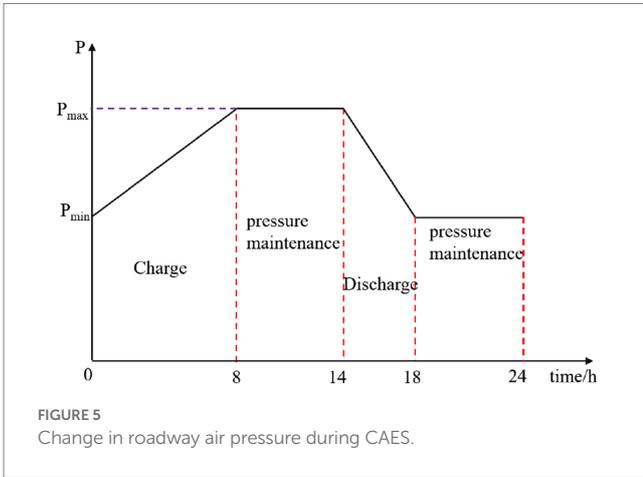
The displacement in a single cycle is related to the mechanical properties of the elastic phase of the surrounding rock. The smaller the upper limit pressure is, the greater the displacement fluctuation in one operating cycle of the roadway roof. The difference in displacement

profile for each cycle is related to the pressure difference. The mechanical properties of the roadway envelope are not completely lost under creep action, and the strain during each air pressure cycle is

related to the stress state. The greater the stress difference is, the greater the displacement amplitude in a single cycle. At a lower pressure limit of 3.0 MPa, the displacement fluctuation at the top of the roadway was approximately 4 mm, whereas at a lower pressure limit of 5.25 MPa, the displacement fluctuation in a single cycle was less than 0.2 mm.

3.3. First principal stress

In the field of underground geotechnical engineering, the first principal stress is generally used to represent the stresses in the rock mass. Figure 8 shows the first principal stress distribution after 10 years of operating the CAES under different conditions. The range of influence of the LLAP on the main stresses in the roadway envelope and the magnitude of the influence both vary. At a lower limit stress of 3 MPa, the surrounding rock stress on the inner surface of the roadway exceeds 10 MPa, with the stress in a 3 m radius of the roadway being approximately 8 MPa. As the lower stress limit is gradually increased, the stress intensity and influence range of the inner surface

FIGURE 5
Change in roadway air pressure during CAES.

FIGURE 6
Displacement clouds after 10 years of CAES in the roadways (**A:** 3 MPa, **B:** 3.75 MPa, **C:** 4.5 MPa, and **D:** 5.25 MPa).

of the roadway decrease. At an LLAP of 5.25 MPa, the stress on the inner surface of the roadway does not exceed 9 MPa, and the area of influence is within 1 m. High-pressure air inside the roadway has an

expansive effect on the roadway. Therefore, the internal pressure of the high-pressure air can reduce the stress concentration in the surrounding rock: the higher the lower limit pressure, the closer the stress distribution in the surrounding rock of the roadway is to the *in-situ* stress and the better the geological stability of the roadway.

3.4. Plastic zone

In the field of underground geotechnical engineering, the Mohr–Coulomb criterion is widely utilised for discriminatory purposes. When the stress on the surrounding rock exceeds a certain value, plastic failure of the surrounding rock will occur. Figure 9 shows the plastic zone distribution after 10 years of CAES in roadways at different lower limit pressures. Noticeably, the distribution pattern of the plastic zone is largely the same, with the plastic zone occurring in almost equal proportions in all directions of the roadway: however, the difference is in the plastic zone volume.

Similarities in plastic zone distribution patterns indicate that the roadways will produce plastic damage under different lower-limit pressure conditions. In roadways buried to a 300 m depth, plastic damage
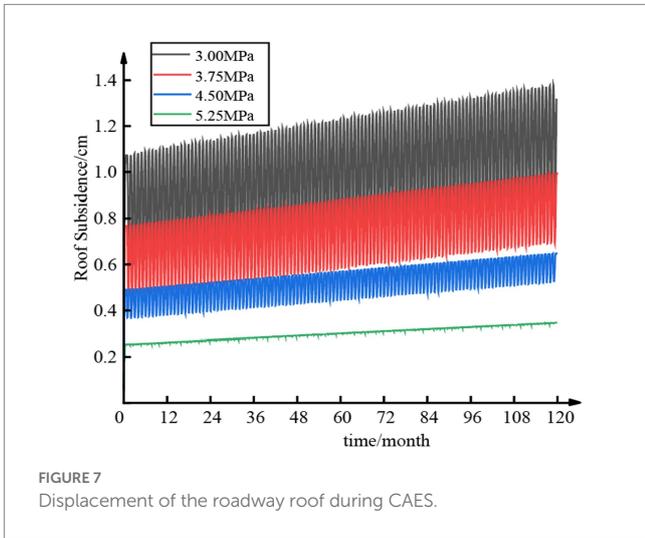

FIGURE 7
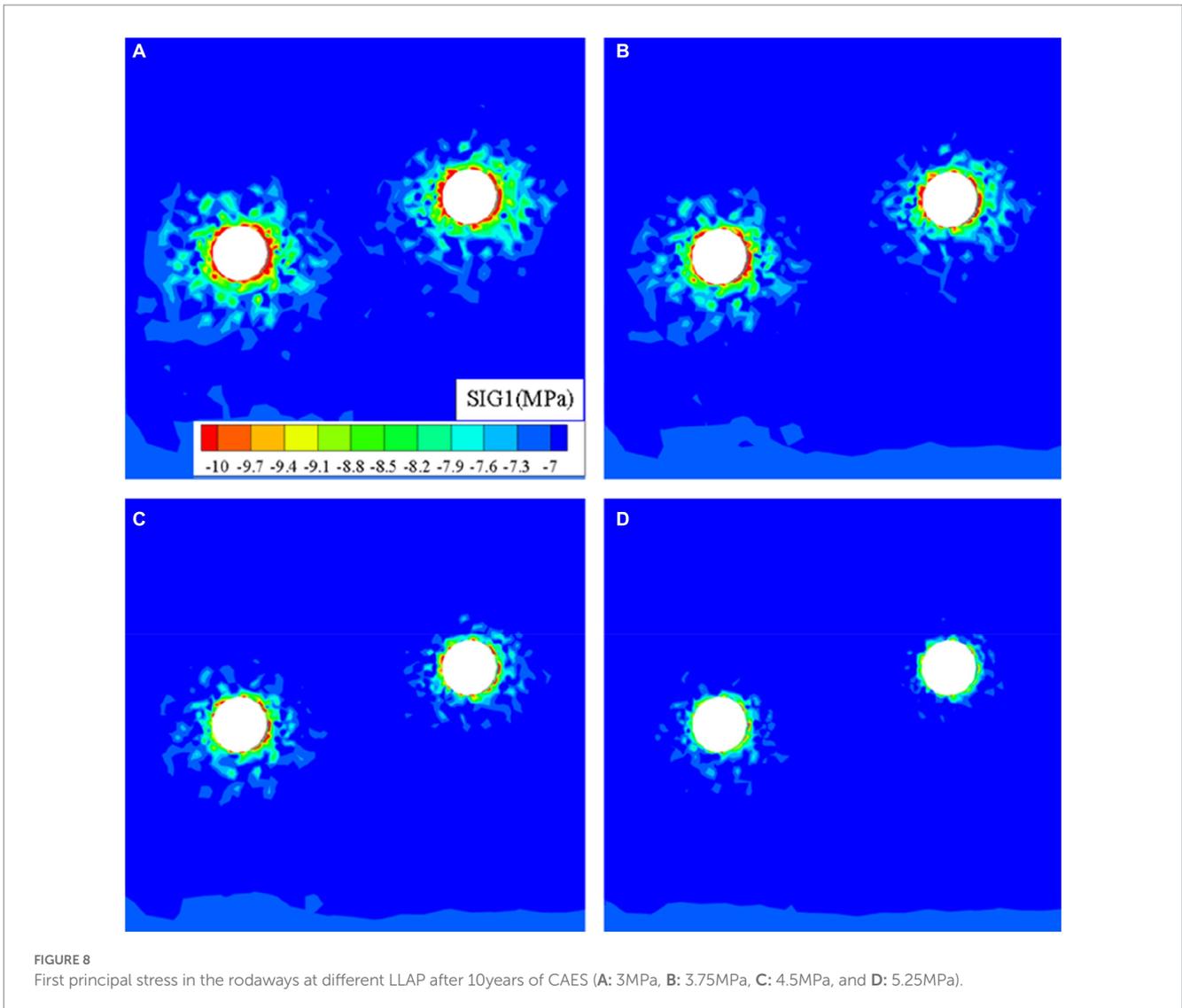Displacement of the roadway roof during CAES.

FIGURE 8
First principal stress in the rodaways at different LLAP after 10years of CAES (**A:** 3MPa, **B:** 3.75MPa, **C:** 4.5MPa, and **D:** 5.25MPa).
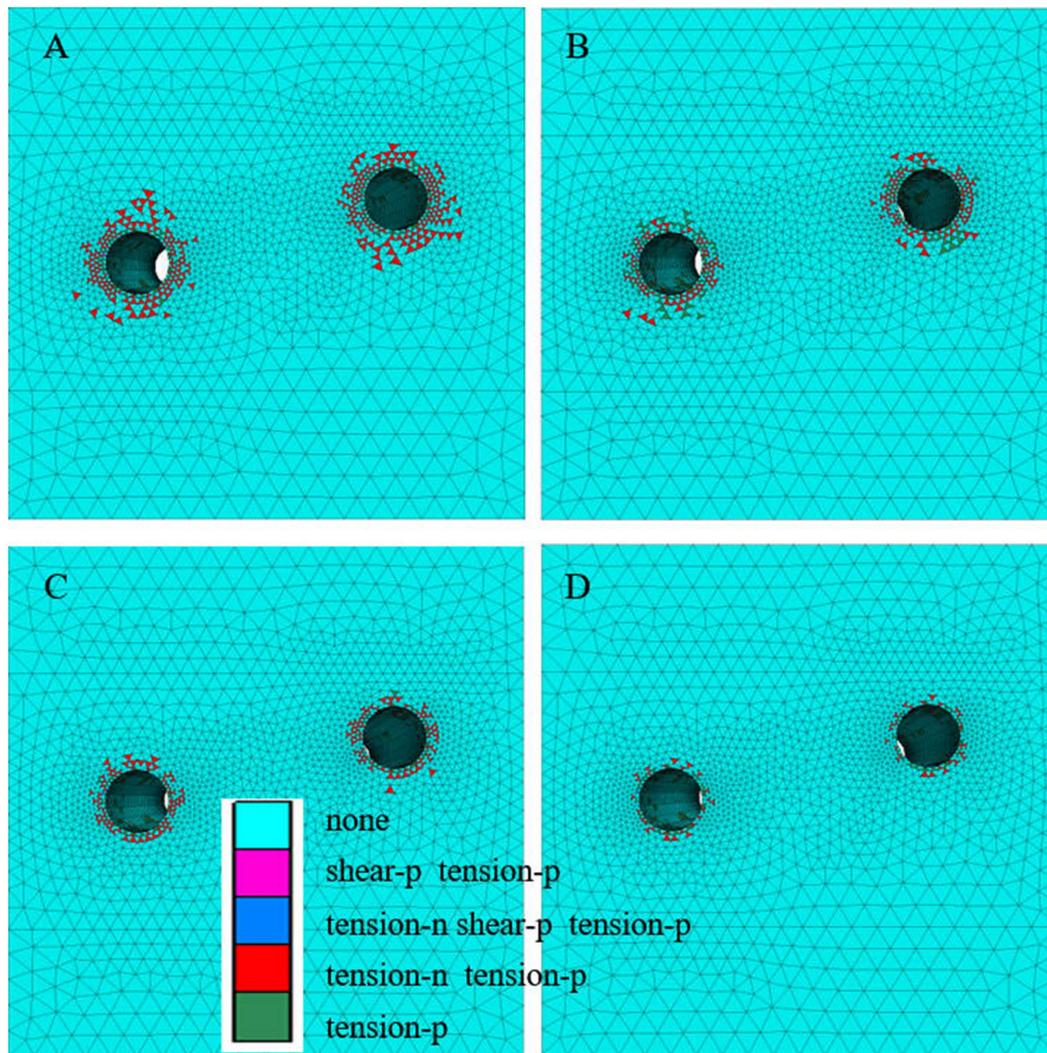
FIGURE 9
Distribution of roadway plastic zones after 10years CAES in different LLAP (**A:** 3MPa, **B:** 3.75MPa, **C:** 4.5MPa, and **D:** 5.25MPa).

can occur even though the unbalance force is much less than the strength of the roadway envelope, which makes it impossible to ignore the damage caused by long-term creep to the roadways envelope even at low stresses when constructing actual air storage roadways. A lower limit pressure of 3 MPa produces the largest plastic zone volume in the borehole envelope, which still occurs beyond double the envelope radius. At 3.75 MPa and 4.5 MPa, the plastic zone is mainly located at half the surrounding rock radius. At a lower limit pressure of 5.25 MPa, the plastic zone is mainly located from 20% to 25% of the surrounding rock radius. A smaller LLAP weakens the ability of the roadway to resist *in-situ* stress, increasing the roadway displacement and plastic zone size. To avoid greater plastic damage deteriorating the air storage stability of the roadway, the lower-limit pressure of the roadway air storage should be maximised.

4. Conclusion

To investigate the effect of LLAP on the stability of CAES in abandoned coal mine roadways, numerical simulation studies have been carried out for a variety of operating conditions. The numerical simulation results reveal that the stability of the roadway changes after 10 years of CAES plant operation while the upper air pressure remains constant, and the variability across different working conditions is large. The main findings from the study are as follows.

1. The larger the LLAP is, the smaller the overall deformation of the roadway. When the LLAP is 3 MPa, the deformation range is approximately 1.3 cm, and when the LLAP is 5.25 MPa, it is only 2 mm.
2. The smaller the LLAP is, the greater the roof subsidence and displacement fluctuation during each air pressure cycle.
3. The first principal stress distribution in the strata near the roadway envelope is negatively correlated with LLAP due to the expansion effect of high-pressure air on the roadway.
4. The plastic zone distributions under different lower limits of air pressure are similar. However, the sizes differ. The influence range of the plastic zone at an LLAP of 3 MPa is approximately 5 times that of an LLAP of 5.25 MPa.

5. In constructing a CAES plant from an abandoned coal mine roadway, the lower limit pressure of compressed air should be appropriately increased to improve the roadway stability.

The conclusions are of some guidance for the construction of CAES plant in abandoned coal mines in Chongqing. Although the creep data is derived from the widely accepted Goodman, the parameters of different types of concrete vary considerably with the development of construction materials. Therefore, in future research, the mechanical parameters as well as the deformation parameters of different types of concrete should be studied and discussed in detail.

Data availability statement

The raw data supporting the conclusions of this article will be made available by the authors, without undue reservation.

Author contributions

JJ: manuscript writing and data processing. PG: analysis of numerical simulation results, image processing, and data collation. XY: experimental programme design and simulation model building. QL: manuscript review and correction. ZL: financial support. JTW: on-site data collection. JXW: experimental protocol design and optimisation. All authors contributed to the article and approved the submitted version.

Conflict of interest

JJ, XY, ZL, and JXW were employed by the East China Electric Power Design Institute Co., Ltd. of China Power Engineering Consulting Group Co., Ltd. QL was employed by the Engineering Technology Institute for Energy Storage of China Power Engineering Consulting Group Co., Ltd.

The remaining authors declare that the research was conducted in the absence of any commercial or financial relationships that could be construed as a potential conflict of interest.

Publisher's note

All claims expressed in this article are solely those of the authors and do not necessarily represent those of their affiliated organizations, or those of the publisher, the editors and the reviewers. Any product that may be evaluated in this article, or claim that may be made by its manufacturer, is not guaranteed or endorsed by the publisher.

References

Apostolou, D., and Enevoldsen, P. (2019). The past, present and potential of hydrogen as a multifunctional storage application for wind power. *Renew. Sust. Energ. Rev.* 112, 917–929. doi: 10.1016/j.rser.2019.06.049

Chen, J., Liu, W., Jiang, D., Zhang, J., Ren, S., Li, L., et al. (2017). Preliminary investigation on the feasibility of a clean CAES system coupled with wind and solar energy in China. *Energy* 127, 462–478. doi: 10.1016/j.energy.2017.03.088

Cui, C.-Q., Wang, B., Zhao, Y. X., and Xue, L. M. (2020). Waste mine to emerging wealth: innovative solutions for abandoned underground coal mine reutilization on a waste management level. *J. Clean. Prod.* 252:119748. doi: 10.1016/j.jclepro.2019.119748

Fan, J., Jiang, D., Liu, W., Wu, F., Chen, J., and Daemen, J. J. (2019). Discontinuous fatigue of salt rock with low-stress intervals. *Int. J. Rock Mech. Min. Sci.* 115, 77–86. doi: 10.1016/j.ijrmms.2019.01.013

Fan, J., Liu, W., Jiang, D., Chen, J., Tiedeu, W. N., and Daemen, J. J. K. (2020). Time interval effect in Triaxial discontinuous cyclic compression tests and simulations for the residual stress in rock salt. *Rock Mech. Rock. Eng.* 53, 4061–4076. doi: 10.1007/s00603-020-02150-y

Fan, J., Liu, P., Li, J., and Jiang, D. (2020a). A coupled methane/air flow model for coal gas drainage: model development and finite-difference solution. *Process Saf. Environ. Prot.* 141, 288–304. doi: 10.1016/j.psep.2020.05.015

Fan, J., Xie, H., Chen, J., Jiang, D., Li, C., Ngaha Tiedeu, W., et al. (2020b). Preliminary feasibility analysis of a hybrid pumped-hydro energy storage system using abandoned coal mine goafs. *Appl. Energy* 258:114007. doi: 10.1016/j.apenergy.2019.114007

Gao, R., Wu, F., Zou, Q., and Chen, J. (2022). Optimal dispatching of wind-PV-mine pumped storage power station: a case study in Lingxin coal mine in Ningxia Province, China. *Energy* 243:123061. doi: 10.1016/j.energy.2021.123061

Goodman, RE. *Introduction to rock mechanics*, Vol. *2*. New York: Wiley; (1989).

Guerra, O. J., Zhang, J., Eichman, J., Denholm, P., Kurtz, J., and Hodge, B. M. (2020). The value of seasonal energy storage technologies for the integration of wind and solar power. *Energy Environ. Sci.* 13, 1909–1922. doi: 10.1039/D0EE00771D

He, Y., Jiang, D., Chen, J., Liu, R., Fan, J., and Jiang, X. (2019). Non-monotonic relaxation and memory effect of rock salt. *Rock Mech. Rock. Eng.* 52, 2471–2479. doi: 10.1007/s00603-018-1718-4

Kang, Y., Fan, J., Jiang, D., and Li, Z. (2020). Influence of geological and environmental factors on the reconsolidation behavior of fine granular salt. *Nat. Resour. Res.* 30, 805–826. doi: 10.1007/s11053-020-09732-1

Kim, H.-M., Rutqvist, J., Ryu, D. W., Choi, B. H., Sunwoo, C., and Song, W. K. (2012). Exploring the concept of compressed air energy storage (CAES) in lined rock caverns at shallow depth: a modeling study of air tightness and energy balance. *Appl. Energy* 92, 653–667. doi: 10.1016/j.apenergy.2011.07.013

Li, Z., Yang, Z., Fan, J., Fourmeau, M., Jiang, D., and Nelias, D. (2022a). Fatigue mechanical properties of salt rocks under high stress plateaus: the interaction between creep and fatigue. *Rock Mech. Rock. Eng.* 55, 6627–6642. doi: 10.1007/s00603-022-02983-9

Li, Z., Yang, F., Fan, J., Jiang, D., and Ambre, J. (2022b). Fatigue effects of discontinuous cyclic loading on the mechanical characteristics of sandstone. *Bull. Eng. Geol. Environ.* 81:336. doi: 10.1007/s10064-022-02837-2

Liu, W., Jiang, D., Fan, J., Chen, J., and Ngaha, W. T. (2023). Energy dissipation of ordinary concrete under discontinuous cyclic compression loading and numerical simulation of the residual stress. *J. Mater. Civ. Eng.* 35:04023142. doi: 10.1061/JMCEE7.MTENG-14804

Liu, W., Peng, H., Guo, P., Chen, S., Liu, W., and Kang, Y. (2022). Experimental study on the mechanical and permeability properties of lining concrete under different complex stress paths. *Front. Earth Sci.* 10:41. doi: 10.3389/feart.2022.810115

Liu, W., Zhang, Z., Chen, J., Jiang, D., Wu, F., Fan, J., et al. (2020). Feasibility evaluation of large-scale underground hydrogen storage in bedded salt rocks of China: a case study in Jiangsu province. *Energy* 198:117348. doi: 10.1016/j.energy.2020.117348

Liu, W., Zhang, Z., Fan, J., Jiang, D., Li, Z., and Chen, J. (2020). Research on gas leakage and collapse in the cavern roof of underground natural gas storage in thinly bedded salt rocks. *J. Energy Storage* 31:101669. doi: 10.1016/j.est.2020.101669

Lund, H., and Salgi, G. (2009). The role of compressed air energy storage (CAES) in future sustainable energy systems. *Energy Convers. Manag.* 50, 1172–1179. doi: 10.1016/j.enconman.2009.01.032

Luo, P., and Chen, N. (2011). Abandoned coal mine tunnels: future heating/power supply centers. *Min. Sci. Technol.* 21, 637–640. doi: 10.1016/j.mstc.2011.10.011

Lutyński, M. (2017). An overview of potential benefits and limitations of compressed air energy storage in abandoned coal mines. *IOP Conf. Ser.* 268:012006. doi: 10.1088/1757-899X/268/1/012006

Ma, G., Xie, Y., Long, G., Tang, Z., Zhou, X., Zeng, X., et al. (2022). Mesoscale investigation on concrete creep behaviors based on discrete element method. *Constr. Build. Mater.* 342:127957. doi: 10.1016/j.conbuildmat.2022.127957

Mahlia, T. M. I., Saktisahdan, T. J., Jannifar, A., Hasan, M. H., and Matseelar, H. S. C. (2014). A review of available methods and development on energy storage; technology update. *Renew. Sust. Energ. Rev.* 33, 532–545. doi: 10.1016/j.rser.2014.01.068

Mathiesen, B. V., Lund, H., and Karlsson, K. (2011). 100% renewable energy systems, climate mitigation and economic growth. *Appl. Energy* 88, 488–501. doi: 10.1016/j.apenergy.2010.03.001

Menéndez, J., Ordóñez, A., Álvarez, R., and Loredo, J. (2019). Energy from closed mines: underground energy storage and geothermal applications. *Renew. Sust. Energ. Rev.* 108, 498–512. doi: 10.1016/j.rser.2019.04.007

Menéndez, J., Ordónez, A., Fernández-Oro, J. M., Loredo, J., and Díaz-Aguado, M. B. (2020). Feasibility analysis of using mine water from abandoned coal mines in Spain for heating and cooling of buildings. *Renew. Energy* 146, 1166–1176. doi: 10.1016/j.renene.2019.07.054

Pfeiffer, W. T., Witte, F., Tuschy, I., and Bauer, S. (2021). Coupled power plant and geostorage simulations of porous media compressed air energy storage (PM-CAES). *Energy Convers. Manag.* 249:114849. doi: 10.1016/j.enconman.2021.114849

Qin, C., and Loth, E. (2021). Isothermal compressed wind energy storage using abandoned oil/gas wells or coal mines. *Appl. Energy* 292:116867. doi: 10.1016/j.apenergy.2021.116867

Ran, Q., Liang, Y., Zou, Q., Hong, Y., Zhang, B., Liu, H., et al. (2023). Experimental investigation on mechanical characteristics of red sandstone under graded cyclic loading and its inspirations for stability of overlying strata. *Geomech. Geophys.* 9:11. doi: 10.1007/s40948-023-00555-x

Schmidt, F., Menéndez, J., Konietzky, H., Pascual-Muñoz, P., Castro, J., Loredo, J., et al. (2020). Converting closed mines into giant batteries: effects of cyclic loading on the geomechanical performance of underground compressed air energy storage systems. *J. Energy Storage* 32:101882. doi: 10.1016/j.est.2020.101882

Wang, M., Guo, P., Dong, W., and Yang, F. (2023). Research on borehole repair model and working parameters optimization of self-propelled rotary excavator. *Front. Earth Sci.* 11:1137946. doi: 10.3389/feart.2022.810115

Wu, D., Wang, J. G., Hu, B., and Yang, S. Q. (2020). A coupled thermo-hydro-mechanical model for evaluating air leakage from an unlined compressed air energy storage cavern. *Renew. Energy* 146, 907–920. doi: 10.1016/j.renene.2019.07.034

Yang, C.-J., and Jackson, R. B. (2011). Opportunities and barriers to pumped-hydro energy storage in the United States. *Renew. Sust. Energ. Rev.* 15, 839–844. doi: 10.1016/j.rser.2010.09.020

Yu, X., and Qu, H. (2010). Wind power in China—opportunity goes with challenge. *Renew. Sust. Energ. Rev.* 14, 2232–2237. doi: 10.1016/j.rser.2010.03.038

Zakeri, B., and Syri, S. (2015). Electrical energy storage systems: a comparative life cycle cost analysis. *Renew. Sust. Energ. Rev.* 42, 569–596. doi: 10.1016/j.rser.2014.10.011

Zhang, N., Lu, X., McElroy, M. B., Nielsen, C. P., Chen, X., Deng, Y., et al. (2016). Reducing curtailment of wind electricity in China by employing electric boilers for heat and pumped hydro for energy storage. *Appl. Energy* 184, 987–994. doi: 10.1016/j.apenergy.2015.10.147

Zhao, X., Cai, Q., Zhang, S., and Luo, K. (2017). The substitution of wind power for coal-fired power to realize China's CO2 emissions reduction targets in 2020 and 2030. *Energy* 120, 164–178. doi: 10.1016/j.energy.2016.12.109

Zhou, S.-W., Xia, C. C., du, S. G., Zhang, P. Y., and Zhou, Y. (2014). An analytical solution for mechanical responses induced by temperature and air pressure in a lined rock cavern for underground compressed air energy storage. *Rock Mech. Rock. Eng.* 48, 749–770. doi: 10.1007/s00603-014-0570-4